instruments

MDPI

Article

Hardware Design of a High Dynamic Range Radio Frequency (RF) Harmonic Measurement System

Ram M. Narayanan [1,*], Kyle A. Gallagher [2], Gregory J. Mazzaro [3], Anthony F. Martone [2] and Kelly D. Sherbondy [2]

1 School of Electrical Engineering and Computer Science, The Pennsylvania State University, University Park, PA 16802, USA
2 U.S. Army Research Laboratory, Sensors Directorate, Adelphi, MD 20783, USA; kyle.a.gallagher3.civ@mail.mil (K.A.G.); anthony.f.martone.civ@mail.mil (A.F.M.); kelly.d.sherbondy.civ@mail.mil (K.D.S.)
3 The Citadel, Department of Electrical & Computer Engineering, Charleston, SC 29409, USA; gmazzaro@citadel.edu
* Correspondence: ram@engr.psu.edu; Tel.: +1-814-863-2602

Received: 15 July 2018; Accepted: 17 August 2018; Published: 19 August 2018

Abstract: Radio frequency (RF) circuit elements that are traditionally considered to be linear frequently exhibit nonlinear properties that affect the intended operation of many other RF systems. Devices such as RF connectors, antennas, attenuators, resistors, and dissimilar metal junctions generate nonlinear distortion that degrades primary RF system performance. The communications industry is greatly affected by these unintended and unexpected nonlinear distortions. The high transmit power and tight channel spacing of the communication channel makes communications very susceptible to nonlinear distortion. To minimize nonlinear distortion in RF systems, specialized circuits are required to measure the low level nonlinear distortions created from traditionally linear devices, i.e., connectors, cables, antennas, etc. Measuring the low-level nonlinear distortion is a difficult problem. The measurement system requires the use of high power probe signals and the capability to measure very weak nonlinear distortions. Measuring the weak nonlinear distortion becomes increasingly difficult in the presence of higher power probe signals, as the high power probe signal generates distortion products in the measurement system. This paper describes a circuit design architecture that achieves 175 dB of dynamic range which can be used to measure low level harmonic distortion from various passive RF circuit elements.

Keywords: high dynamic range measurements; harmonic measurement system; nonlinear distortion; harmonic radar; passive RF components

1. Introduction and Motivation

Nonlinearities in RF and microwave systems can take many forms. Historically, nonlinearities are found in circuit elements such as diodes, transistors, amplifiers, mixers, and others. In addition, nonlinearities have been found in other circuit components and are generated by different mechanisms. One of the less common nonlinear mechanisms is passive intermodulation (PIM) distortion, which occurs in antennas [1,2], cables, connectors [2–4], metal-to-metal junctions [5,6], and various components [7,8]. A recent development has led to the exploitation of nonlinearities in electronic circuits to detect and track nonlinear targets [9–15].

Circuit elements exhibit nonlinear properties either by design or by consequence. By design, P-N junctions, such as diodes, are inherently nonlinear, and this property is exploited for their use in frequency mixers, which are used to upconvert or downconvert signals from one frequency to another.

The operation of mixing two signals together to create a new frequency is a nonlinear operation. By consequence, many RF and microwave circuit elements exhibit unintended nonlinear properties. An example is the RF amplifier. Amplifiers are intended to operate linearly, boosting the input signal without creating extraneous frequencies at the output. In practice, creating a linear amplifier is not possible and additional frequency content is generated that distorts the desired signal. Much research has been done to linearize amplifiers [16–20]. The unintended frequency content generated by the nonlinear properties of the amplifier interferes with other radar and communication systems [21–23], as well as affect the sensitivity of the receiver.

There are other nonlinear effects that are subtler and do not manifest as often. Among these is PIM, which is observed when high power signals interact with components that are weakly nonlinear. Such components do not exhibit measurable nonlinear distortion under normal conditions. In communication systems, the PIM produced can fall close to the fundamental band and interfere with adjacent communication channels [24,25]. To combat this, much research has gone into linearizing communication systems [3,24,26]. For close-in intermodulation distortion (IMD), the frequency separation between the fundamental signal and PIM is too small to effectively filter out. Additionally, the communication channels change frequency quickly to accommodate multiple users. So, adaptable filters with large Q values would be needed; however, reconfigurable, high Q filters do not exist. For this reason, adaptive techniques are used to predict and cancel the nonlinearities. Such techniques include predistortion, feedforward linearization, channel equalization, etc. [27–32].

Measuring weakly nonlinear RF circuit components requires specialized RF hardware [3], which itself must be highly linear and devoid of any self-generated nonlinearities. If the measurement system is not highly linear, the measurements will reflect the distortions caused by the test hardware in addition to the device under test (DUT).

Commercially-available high dynamic range PIM measurement systems are accessible today [33,34]. These systems are typically designed for specific frequencies, usually around the cell band. They use a two-tone test setup and achieve up to 170 dBc of dynamic range using high Q filters that are fixed in frequency, but lack frequency agility. A commercially-available nonlinear vector network analyzer, PNA-X, demonstrates far more flexibility than the fixed frequency PIM testing systems, and has the ability to vary tone spacings and tone amplitudes [35]. The PNA-X system also tracks intermodulation (IM) products and harmonics, keeping track of all the nonlinear terms [36]. However, it lacks the dynamic range necessary to measure nonlinear distortion from weakly nonlinear devices, as they are specified to generate harmonics lower than 60 dBc [37].

Feedforward cancellation systems have been developed that enable close-in PIM to be measured with a 160-dBc dynamic range, measured from the probe signal power to the spurious free IM frequency [16,38–40]. The systems achieve a large dynamic range by taking great care to linearize their measurement system, which requires high levels of isolation between nonlinear circuit elements in the test setup to the DUTs. These systems also employ an adaptable cancellation system that removes the probe signals before PIM measurements are made. The linearization, isolation, and removal of the probe signal are essential to any high dynamic range measurement system. The downside to constructing such a test setup is the complexity of the system. These systems require iterative feedback from the receiver to cancel the fundamental probe signal. They also require an optimization algorithm to maximize the cancellation of the probe signal to maximize the dynamic range of the measurements.

This paper describes an alternate approach to measuring low level nonlinear distortion from weakly nonlinear targets. The measurement system uses the second harmonic to characterize the nonlinearities of passive RF circuit elements. The measurement system achieves the high dynamic range, of the order of 175 dBc, necessary to measure weakly nonlinear devices while covering a 20% bandwidth, something the PNA-X and other commercially-available systems cannot accomplish. The measurement system is also low complexity, not requiring complicated feedforward cancellation circuits.

Section 1 introduces the mathematics required to characterize nonlinearities from circuit elements. Section 2 describes basic harmonic measurement techniques to linearize standard RF instrumentation. Section 3 considers issues in creating a high dynamic range harmonic measurement system. Section 4 discusses the high dynamic range harmonic measurement system constructed that achieves 175 dBc of dynamic range. Section 5 presents the results obtained from the measurement system of various RF system components. Section 6 concludes the paper.

2. Nonlinear Device Modeling and Characterization

To accomplish the goal of characterizing nonlinearities generated by RF circuit components, a nonlinear system model is needed. The model must characterize the nonlinear properties of the devices and predict the behavior of the devices under different conditions. Having the ability to predict the nonlinear response of weakly nonlinear devices enables a system designer to better predict how much distortion will be present in the system. Therefore, the input-output relationship for nonlinear devices needs to be defined.

In general, nonlinear systems do not satisfy the linearity property, i.e., superposition and scaling properties. The output of nonlinear systems contains signals that cannot be represented as a linear combination of the input signals. These signals can be at different frequencies than the input frequencies. In this paper, nonlinear systems are modeled using the power series [7,8,41–43], which is represented as

$$y = \sum_{n=0}^{\infty} y_n = \sum_{n=0}^{\infty} a_n x^n, \tag{1}$$

where x is the input signal, y is the output signal, and a_n is the scale factor coefficient of the nth order nonlinearity.

When the input to a nonlinear system is a single frequency, the output consists of harmonics of that frequency occurring at integer multiples of the fundamental frequency. With a single frequency input to the power series given by $x = x_0 \cos(\omega_0 t + \theta)$, the output can be shown to be [44]

$$y = \sum_{n=0}^{\infty} c_n x_0^n \cos(n\omega_0 t + n\theta). \tag{2}$$

The amplitude of the frequency domain representations of Equation (2) is illustrated graphically in Figure 1. Generally, the output amplitude drops as the harmonic order n increases.

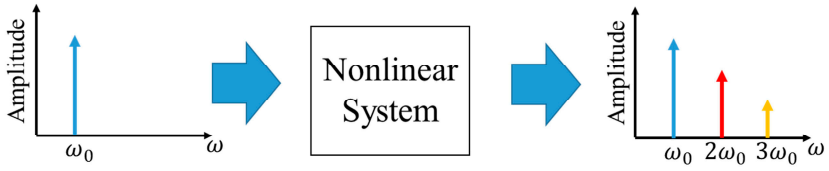

Figure 1. Illustration of the output due to a single frequency input into a nonlinear system.

Equation (2) expresses the nonlinear system input-output relationship in terms of voltage. Engineers typically prefer to use power units; therefore, the voltage expression is converted to power. The average power of a sinusoidal signal is given by $P_{\text{ave}} = V_{\text{peak}}^2/2Z_0$, where V_{peak} is the peak voltage and Z_0 is the system characteristic impedance. Thus, the power in the harmonics can be represented in a decibel (dB) scale as:

$$P_{\text{out},n}[\text{dBm}] = nP_{\text{in}}[\text{dBm}] + D_n, \tag{3}$$

where $P_{\text{out},n}$ is the output power at the nth harmonic, P_{in} is the input power at the fundamental frequency ($n = 1$), D_n is a coefficient expressed in $\text{dBm}^{(1-n)}$, and dBm represents power expressed in decibels relative to one milliwatt.

The implications of Equation (3) are that the output-to-input power ratio for the nth harmonic follows an $n:1$ relationship in a dB scale. Therefore, a 1-dB increase in the input creates a 2- and 3-dB increase in output power for the second and third harmonics, respectively. In general, the D_n values are frequency-dependent and characterize the nth order nonlinear properties of a device. A more commonly found characterization of a device's nonlinear properties is its output intersect point OIP_n, which is the intersection point at which the 1:1 slope of the linear response intersects the $n:1$ slope of the nth order nonlinearity. This is shown in Figure 2 for the second harmonic, i.e., $n = 2$.

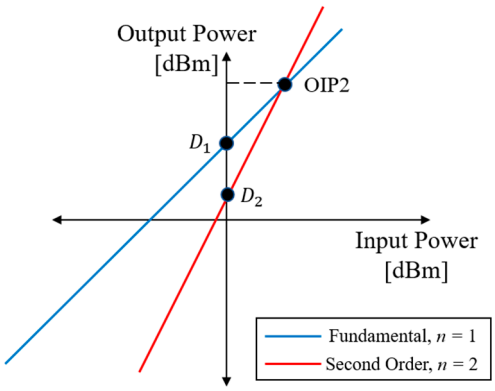

Figure 2. Illustration of the relationship between OIP_2 and D_2.

The relationship between D_n and OIP_n can be found by manipulating Equation (3) to yield:

$$D_n = (1 - n)\text{OIP}_n + nD_1. \tag{4}$$

3. Issues in Creating a High Dynamic Range Harmonic Measurement System

To measure harmonics generated by devices that are not traditionally nonlinear, a high dynamic range (DR) measurement system must be developed. The measurement system must create a highly linear probe signal and must have the ability to measure very weak nonlinear signals in the presence of the large fundamental probe signal.

There are two important aspects of designing a high DR harmonic measurement system: (1) the use of a high DR receiver to measure the weak nonlinear signals in the presence of the high power probe signal; and (2) generation of a highly linear probe single used to probe a DUT. Both the receiver and probe single generator have their unique problems that must be addressed to generate high fidelity, linearized signals. This section addresses these problems.

3.1. Creating a Highly Linear Harmonic Receiver

The first problem in creating a highly linear harmonic receiver is that the measurement hardware is itself nonlinear. The RF front end of a spectrum analyzer consists of nonlinear devices such as amplifiers and mixers. For the results presented in this paper, a National Instruments (NI) (Austin, TX, USA) PXIe-5668R spectrum analyzer is used. The 5668R is specified to generate a second harmonic >69 dBc down from the fundamental, between 700 to 1000 MHz with 0-dBm input power [45]. Although the data sheet specifies >69 dBc, the measured self-generated second harmonic is 80 dBc. This 80 dBc of dynamic range is sufficient to make harmonic measurements of strongly nonlinear devices, such as amplifiers, mixers, and diodes, but is inadequate to make measurements of weakly nonlinear elements. The first example of this shown in Figure 3, which depicts an ideal probe signal entering an amplifier. In Figure 3, "DUT" stands for "device under test", "HPF" stands for "high-pass filter", and "LPF" stands for "low-pass filter". The DUT is a Mini-Circuits amplifier ZX60-3018G-S+. The fundamental and harmonic responses are made on the PXIe-5668R spectrum analyzer. The choice of filters is very important in architecting a reliable harmonic measurements system [46].

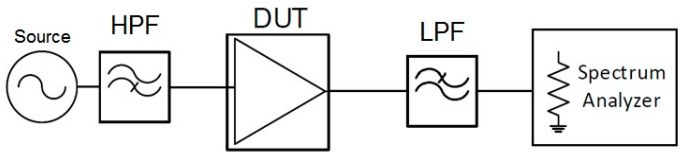

Figure 3. Measuring the second harmonic output of an amplifier using an ideal linear source.

Three different low-pass filter options are tested using the setup in Figure 3. These include: (1) no filter; (2) a Mini-Circuits reflective filter VLF-1200; and (3) a Mini-Circuits diplexer RPB-272. When no filter is used, the dynamic range of the test setup is set by the spectrum analyzer, namely 80 dBc. The dynamic range of test setup is increased by filtering out the fundamental frequency before it enters the spectrum analyzer. For every 1-dB attenuation of the fundamental, the self-generated second harmonic of the spectrum analyzer decreases 2 dB. This follows from the relationship in Equation (3). A commercial off-the-shelf (COTS) Mini-Circuits high-pass filter VHF-1200 would be a natural choice, but most COTS filters attenuate the stop band frequencies by creating an impedance mismatch. The result of the mismatch is that the undesired frequencies are reflected and not passed through the filter. The impact of this is examined later. To attenuate the fundamental frequency and to reduce the reflection back into the DUT, a diplexer is used. The low frequency port is terminated in 50 Ω. For this setup, the probe signal is set to 800 MHz and the probe signal power is calibrated to be −20 dBm at the input to the amplifier.

The resolution bandwidth (RBW) on the spectrum analyzer was set to 800 Hz and the internal attenuator was set to 30 dB. The results in Table 1 illustrate the following two concepts: (1) the spectrum analyzer has the dynamic range to measure the second harmonic response from the Mini-Circuits amplifiers; and (2) the reflective filter alters the test setup and yields false results. If the input power to the spectrum analyzer is 0 dBm, the spectrum analyzer will generate a second harmonic on the order of −90 dBm. Therefore, the reading of −36.3 dBm is well above the self-generation level of the setup and it is a valid reading.

Table 1. Filter testing results to improve dynamic range.

Filter Type	Power at 800 MHz	Power at 1600 MHz
None	−0.3 dBm	−36.3 dBm
Reflective	−39.3 dBm	−29.5 dBm
Diplexer	−42.6 dBm	−38.6 dBm

To measure lower level harmonics, the dynamic range of the system needs to be increased. This can be done by using a filter. When a reflective filter is used, the undesired probe signal is reflected causing a reverse traveling wave that enters the output port of the DUT. Once the probe signal enters the output port of the DUT, the probe signal generates additional nonlinearities. The results in Table 1 show more than a 7-dB increase in the measured second harmonic when the reflective filter is used. Figure 4 illustrates this reflection and additional generation of the second harmonic when a reflective filter is used.

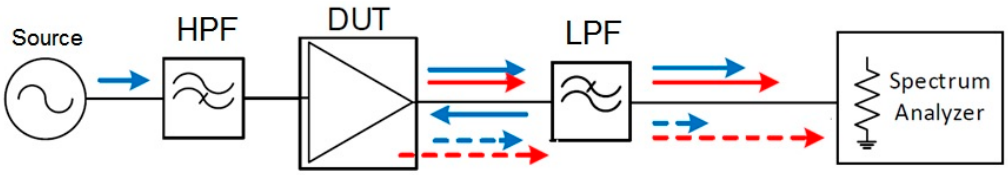

Figure 4. Measuring the second harmonic output of an amplifier with a reflective filter showing errors in the measurement setup.

In Figure 4, the blue lines represent the probe signal at fundamental frequency, the red lines represent the second harmonic signal, and the dashed lines represent the signals that are generated by the reflected probe signal. For the measurements taken in Table 1, the setup was calibrated to remove the cable loss and the loss through the filter at the second harmonic. The VHF-1200 and RBF-272 were chosen to have similar losses at 800 and 1600 MHz, the fundamental frequency of the probe signal and its second harmonic under test, respectively. The return loss (S_{11}) for both the VHF-1200 and RBF-272 are shown in Figure 5.

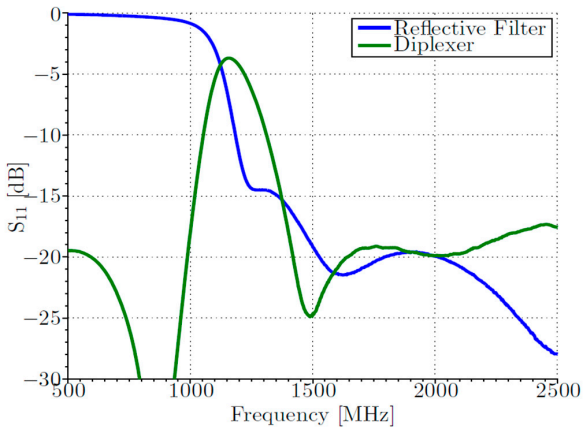

Figure 5. S-parameters of the Mini-Circuits VHF-1200 high-pass filter and RBF-272 diplexer in the high pass configuration.

Although the high-pass filter is not needed for this amplifier example, filtering is needed to increase the dynamic range to greater than 160 dBc, the dynamic range needed to measure nonlinearities from passive circuit components. The amount of attenuation needed to achieve a desired dynamic range of DR_d with a current dynamic range of DR_c is given by:

$$A_H = \frac{\mathrm{DR}_d - \mathrm{DR}_c + 10}{2}, \tag{5}$$

where A_H is the attenuation needed by the high pass filter at the fundamental frequency. The expression is given in a dB scale. An extra 10 dB is added to the desired dynamic range to ensure that the self-generated nonlinearities are at least a factor of 10 less than the desired minimum detectable nonlinearity. Equation (5) also predicts that the dynamic range is increased by 2 dB for every 1 dB of attenuation in the high-pass filter.

This section has demonstrated the importance of properly linearizing the receive section of a harmonic measurement system. In this section, it was assumed that the probe signal was ideal, i.e., it contained no measurable second harmonic. The next section shows how to ensure proper linearization of the probe signal and illustrates a potential issue when constructing the measurement setup.

3.2. Creating a Harmonic Free Probe Signal

In the previous section, it was assumed that the probe signal was ideal, i.e., it contained no second harmonic. This is not physically possible and this section demonstrates how to create a probe signal that is "ideal enough" to measure weakly nonlinear targets. In the previous section, the fundamental frequency needed to be attenuated in the receiver to measure the second harmonic accurately. In this section, the second harmonic must be removed from the probe to ensure that the measured harmonic is coming solely from the DUT and not the probe signal. If the second harmonic is not adequately attenuated from the probe signal, the measurement system generates a false, self-created second harmonic. This problem is viewed as co-site interference.

3.2.1. Filter Considerations

The amount of second harmonic present in probe signal can never reach zero, or $-\infty$ dB. Therefore, it can only be attenuated to the noise floor of the measurement setup. As in Section 3.1, the linearity of the measurement system can be increased by filtering. The NI PXI-5651 signal generator used is specified to produce less than 25 dBc of second harmonic when the output power is 0 dBm [47]. We assumed this value does not change too much when the output power is increased to +10 dBm. With +10 dBm of output power, the 5651 signal generator will produce less than -15 dBm of second harmonic, thereby providing 25 dBc of dynamic range. Thus, if this generator is used without any filtering, accurate second harmonic measurements are made to -5 dBm, including the 10-dB safety factor for signal-to-interference ratio, which is not very useful when trying to make sensitive harmonic measurements. To increase the dynamic range of the receiver, a low-pass filter is used. For the probe signal, the improvement in dynamic range is a 1:1 ratio. So, if the signal generator provides a 25-dBc dynamic range and 160 dBc is desired, the attenuation required for the low pass filter is 145 dB. The general expression for the attenuation needed by the low pass filter is:

$$A_L = \mathrm{DR}_d - \mathrm{DR}_g + 10 \tag{6}$$

where A_L is the attenuation required of the low-pass filter at the second harmonic and DR_g is the dynamic range of the signal generator. Again, a 10-dB safety factor is built in to ensure 10 dB of signal-to-interference ratio.

Most COTS filters do not provide greater than 100 dB of attenuation required to linearize the probe signal. Therefore, multiple filters need to be cascaded to achieve the large attenuation required. As stated in Section 3.1, most COTS filters are reflective, and attenuation is achieved in the stop band by an impedance mismatch causing the stop band frequencies to reflect backwards and not pass through it. This reflective nature of filters causes problems.

The Mini-Circuits low-pass filter, Model # VLF-1200, has a cut off frequency of 1 GHz. However, the stop band of this filter does not meet the >100-dB attenuation requirement. Therefore, multiple filters need to be cascaded to increase the stop band attenuation. Figure 6 shows the measured and theoretical $|S_{21}|$ response when two VLF-1200 filters are cascaded. The theoretical cascaded $|S_{21}|$ response was computed as a product of the individual $|S_{21}|$ responses.

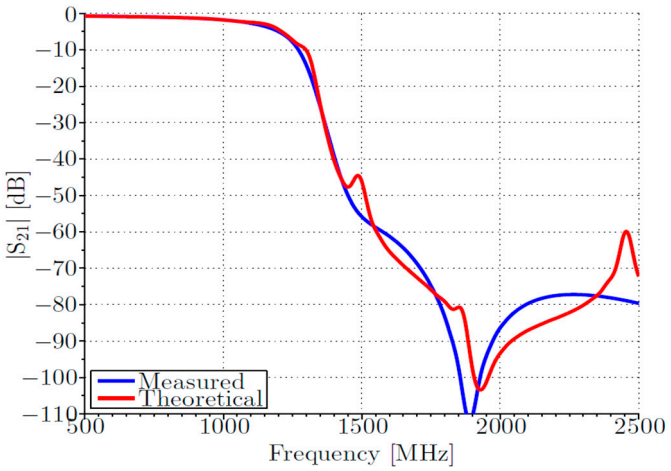

Figure 6. Measured and theoretical $|S_{21}|$ response when two VLF-1200 low-pass filters are cascaded.

When the two reflective low-pass filters are cascaded, the measured and theoretical responses do not closely match. This point is further investigated in [48], where three reflective low pass filters are cascaded. The measured results when three low-pass filters are cascaded show more discrepancy when compared to the theoretical response.

Using a number of cascaded reflective filters causes large variations in the measurement system's dynamic range as a function of frequency. If the measurement system operates at a single frequency, a null in the cascaded frequency response can be used. If measurements are taken over a bandwidth of frequencies, the fluctuations in the frequency response would not permit reliable, repeatable, and accurate measurements.

3.2.2. Diplexer Considerations

This leads us to the choice of microwave diplexers for accomplishing the filtering operation. Diplexers are three-port devices which separate power entering a common input into two frequency bands; or conversely, they combine two frequency bands arriving separately into a common output [49]. Diplexers in which there are adequate guard bands between channels may be designed by suitably connecting two separate, doubly-terminated filters onto a T-junction. These devices are typically employed to connect the transmit and receive filters of a transceiver to a single antenna through a suitable three-port junction [50,51]. Diplexers are designed to have low PIM and, therefore, will have low harmonic distortion. With that said, they will generate their own harmonics, but these will be very low, on the order of high-quality cables and connectors, i.e., <-170 dBc. The harmonics generated by the diplexers, cables, and connectors will set a fundamental limit on the dynamic range of the system.

As such, they have the ability to be configured differently for different applications. Diplexers can be used as a low-pass filter by terminating the high frequency port in 50 Ω and using the common port and low frequency port. Unlike reflective filters, diplexers can be cascaded to increase their stop band attenuation. To cascade diplexers in a low-pass configuration, we terminate the high frequency port and connect the common port to the low-pass port of the next diplexer. By connecting the low-frequency port of one diplexer to the common port of another diplexer, the reflections between cascaded diplexers is reduced, when compared to the reflections when reflective filters are cascaded. By terminating the high-frequency port, the stop band frequencies have a path to 50 Ω and the cascaded network is well-behaved. Figure 7 shows the $|S_{21}|$ response when two diplexers are cascaded in a low-pass configuration.

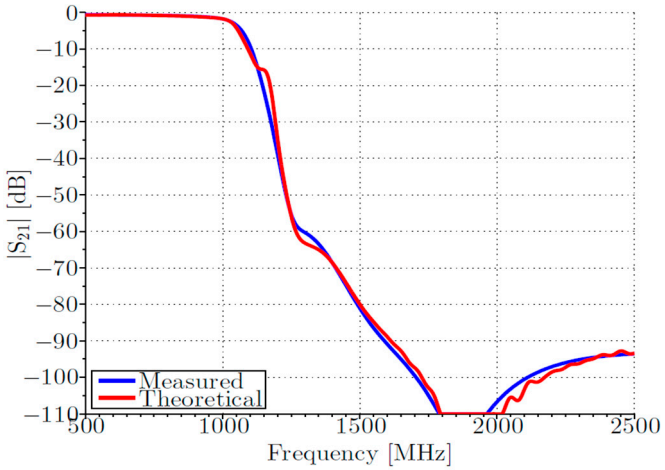

Figure 7. Measured and theoretical $|S_{21}|$ response when two RBF-272 diplexers in low-pass filter configuration are cascaded.

Figure 7 shows that when two diplexers are cascaded, the measured $|S_{21}|$ closely matches the theoretical response. Comparing Figures 6 and 7, we note that cascading diplexers is more desirable than cascading reflective filters for increasing stop band attenuation.

4. System Hardware Design

Using the information from the previous sections, a higher power, high dynamic range harmonic measurement system was constructed. The measurement system was developed to measure second harmonic, $n = 2$, responses from weakly nonlinear targets. The system also collects data on the linear, fundamental ($n = 1$) responses from DUTs. The system was designed to measure both the pass through and reflected, linear and second harmonic response. This allows for full characterization of devices. The linear frequency range spans 800 to 1000 MHz and the second harmonic frequency range is 1600 to 2000 MHz. A block diagram of the measurement system is shown in Figure 8. Note that the second diplexer is flipped to give the harmonics traveling in the reverse direction a path to a 50-Ω termination. Wherever possible, all inputs and outputs are terminated in 50 Ω at both the fundamental frequency and second harmonic.

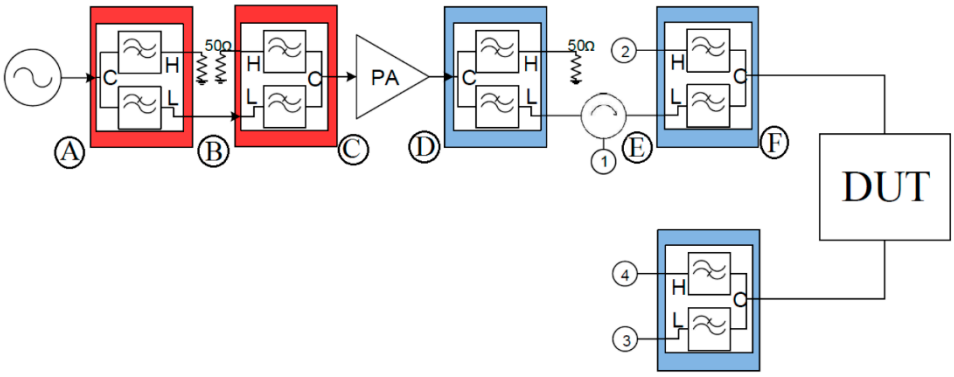

Figure 8. Block diagram of the linear/nonlinear measurement system with specific test locations marked.

A NI PXI-5651 signal generator is used to create the probe signal. Next, Mini-Circuits RBF-272 diplexers are used in a low pass configurations to linearize the probe signal, filter out any second harmonic generated by the signal generator. To boost the power of the probe signal, a ZHL-30W-252-S+ Mini-Circuits power amplifier (PA) is used. The probe signal is amplified to 10 W (+40 dBm). The power amplifier is a nonlinear device and generates significant harmonics that need to filtered. Since the fundamental frequency power is at 10 W, high power custom diplexers, manufactured by Reactel, are used.

The high power diplexers are rated up to 100 W continuous wave input power. They are cavity diplexers that provide greater than 80 dB of rejection in the stop band. The passband attenuation is less than 0.4 dB. Section 3.2 demonstrated the need for a highly linear probe signal; therefore, two such diplexers are cascaded to attenuate the self-generated harmonics below the noise floor. In addition to the diplexers, an isolator is used to isolate the power amplifier output from the DUT and avoid mismatches. The insertion loss of the isolator is 0.2 dB. Thus, the power delivered to the DUT was approximately +39 dBm.

Test results from a single diplexer are presented in Figure 9. The data in Figure 9 show the diplexers' ability to pass the fundamental frequencies, from 800 to 1000 MHz, and attenuate the second harmonics, from 1600 to 2000 MHz.

Figure 9a shows that one cavity diplexer attenuates all harmonics, from 1600 to 2000 MHz, by at least 80 dB with less than 0.4 dB attenuation at the fundamental frequencies, from 800 to 1000 MHz. The high frequency path of the diplexer was also tested and the results are shown in Figure 9b. Again, the diplexer attenuates the unwanted fundamental frequencies (here it is from 800 to 1000 MHz) by more than 80 dB and it passes the desired harmonic frequencies, 1600 to 2000 MHz, with less than 0.4 dB of loss. Since the diplexers have very little loss in the pass band, they do not absorb a significant amount of pass band energy.

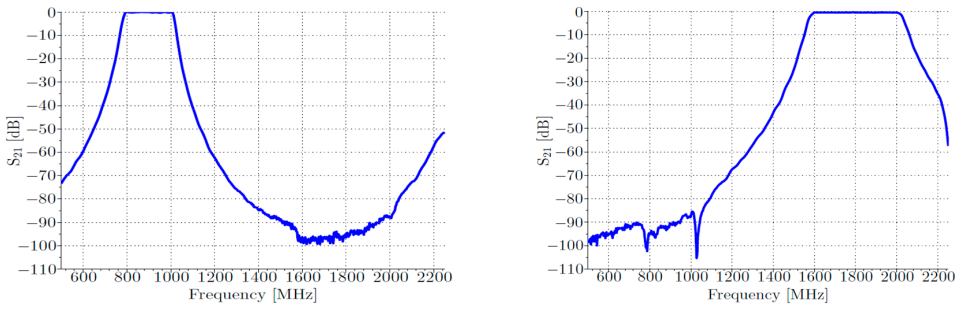

Figure 9. Measured $|S_{21}|$ response for Reactel diplexers for various ports: (**a**) low-frequency port; and (**b**) high-frequency port.

A measured link-budget for a 900-MHz tone, used as the probe signal, is presented in Table 2. Note from Table 2 that going from D to E for the second harmonic shows a loss of 113.4 dB. However, according to Figure 9a, the loss is seen to be around 95 dB. This discrepancy is probably due to the fact that the $|S_{21}|$ measurements are made on a network analyzer and the results in Figure 9a are likely limited by the network analyzer's noise floor or the internal coupling.

Table 2. Measured link-budget for the harmonic distortion measurement system, in dBm, at different locations marked in Figure 8.

Frequency	A	B	C	D	E	F
900 MHz	−7.7	−8.3	−8.9	+40.5	+40.2	+40.1
1800 MHz	−40.8	−94.7	<−130	+22.4	−91	<−130

Photographs of the NI chassis and the RF components (Mini-Circuits and Reactel diplexers and power amplifier) are shown in Figures 10 and 11, respectively.

The receiver hardware is straightforward. The probe signal, at the fundamental frequency, is separated from the second harmonic using another high power diplexer. The fundamental frequency passing through the DUT is measured at port 3 in Figure 11. The output second harmonic is measured at port 4. The spectrum analyzer has an 80-dBc dynamic range; coupling this with the 80-dB of loss provided by the Reactel diplexer yields a system dynamic range of over 200-dBc, according to Equation (5). However, the theoretical 200-dBc dynamic range is unachievable, as in practice, the system would be noise limited before 200-dBc can be achieved. The noise floor of the receiver is measured to be less than 135 dBm. With the probe signal measured to be greater than 40 dBm and the noise floor below 135 dBm, the system's dynamic range is estimated to be greater than 175 dB.

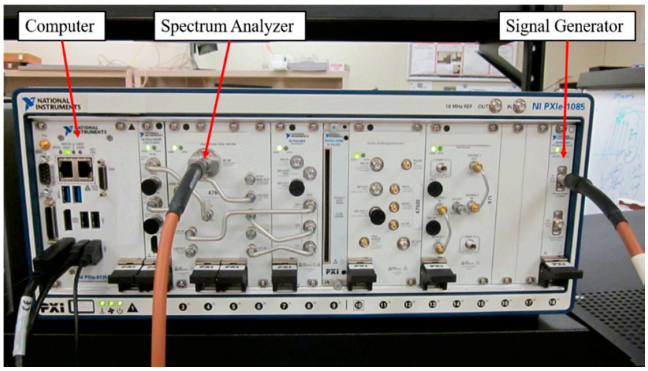

Figure 10. Photographs of the NI chassis with computer, signal generator, and spectrum analyzer.

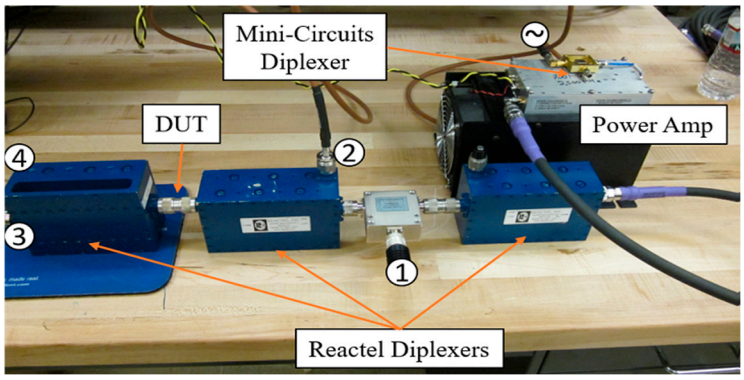

Figure 11. Photograph of the diplexers and 10-W power amplifier.

5. System Test Results

The high dynamic range measurement system described in Section 4 was used to measure the second harmonic response from a variety of circuit elements. The passive devices tested are shown in Figure 12.

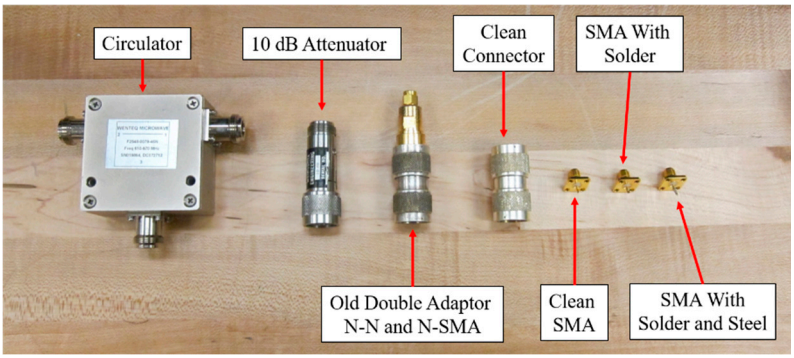

Figure 12. Devices tested for second harmonic characterization.

The two port devices were tested for their input and output harmonic generation while the one-port devices could only be tested for their reflected harmonic generation. Test setups for the harmonic through and harmonic reflection measurements are shown in Figures 13 and 14, respectively.

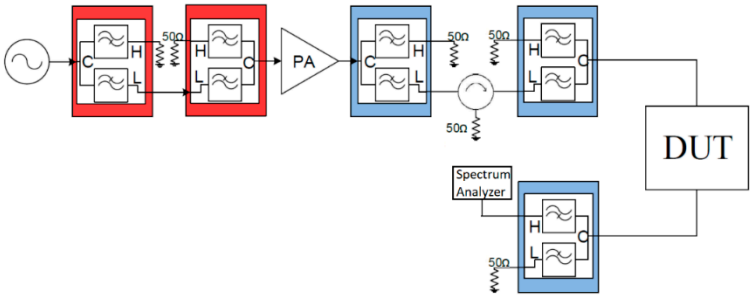

Figure 13. Test setup for harmonic through measurement.

Since the spectrum analyzer only has one input port, the fundamental and second harmonic at the output of the DUT need to be measured via two separate measurements. Therefore, the loading conditions of the two measurements are slightly different. The spectrum analyzer is matched to 50 Ω throughout the bands of interest with an input reflection coefficient $|S_{11}|$ of less than 20 dB,

which provides a 99% power transfer. The differences between the loading conditions for the fundamental and second harmonic measurements is therefore expected to be negligible compared to using a 50 Ω termination. Thus, we believe that any mismatches between the two measurement setups would result in an insignificant difference in nonlinear distortion generated.

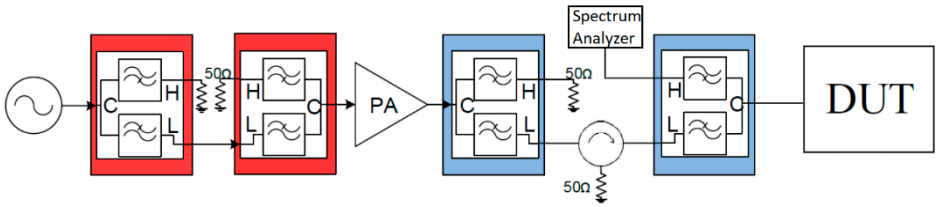

Figure 14. Test setup for harmonic reflection measurement.

The test results are summarized in Table 3. The values are shown for D_2 in Equation (3), the units for which are dBm^{-1}. A lower value, i.e., more negative, indicates better harmonic suppression.

Table 3. Harmonic generation results from various passive devices shown in Figure 12.

Device	$D_{2,\mathrm{ref}}$ (dBm^{-1})	$D_{2,\mathrm{through}}$ (dBm^{-1})
Open circuit	−215.0	—
N(m)-N(m) adaptor (new)	−210.0	−210.0
Mixer	−30.0	−40.0
10-dB attenuator	−153.6	−155.4
Circulator (terminated in 50 Ω)	−121.3	−104.0
Circulator (open-circuited)	−108.4	—
N(m)-SMA(f) adaptor (old)	−190.8	—
Open SMA connector	−202.0	—
Open SMA connector with solder	−196.5	—
Open SMA connector with solder and steel	−174.9	—

The results from the open circuit and new N(m)-N(m) adaptor show the minimum detectable D_2 coefficient the setup can measure. The open circuit and new adaptor test cases are the baseline measurements used for monitoring the spurs created at the second harmonic and the noise floor, which determines the system dynamic range. Any significant contributions from the higher-order harmonics to the second harmonic would be indicated in this measurement. The observations from this measurement indicated that distortion created from these higher order harmonics are below the noise floor.

Since a mixer, by design, is a nonlinear component whose nonlinearity is essential for frequency conversion [52], it shows much higher D_2 values. Attenuators typically consist of resistors connected in T- or ΠΠ-configurations with dissimilar metal contacts, which results in D_2 values of about 60 dB higher than the detection floor. The intense RF magnetic field across the ferrite disk excites nonlinear behavior in a circulator [53], which explains its higher values. The old, i.e., well-used, adaptor shows about 20-dB increase in D_2 compared to the new adaptor, which may be ascribed to possible corrosion caused by wear and tear and environmental effects. Connectors terminated in solder and steel show higher D_2 values compared to the unterminated connector due to the effect of the dissimilar metal contacts, with steel adding about a 20-dB higher value, consistent with the results reported in [54,55]. The mixer serves as a reference for traditionally nonlinear devices. Table 3 shows that the nonlinear response from the mixer is about 90 dB over the circulator, about 120 dB over the attenuator, and about 145–170 dB over the adaptors, at an input of 0 dBm.

6. Conclusions

As the frequency spectrum gets more crowded and the demand for wireless communication increases, nonlinear distortions generated by passive elements become more relevant. Commercially-available nonlinear measurement systems are expensive and either lack the dynamic range needed to make the sensitive measurements or are fixed in frequency and do not provide the flexibility required. Robust feed-forward systems have been constructed that provide both the flexibility and dynamic range needed to made the sensitive measurements, but these systems are complex and require iterative tuning and optimization algorithms. This paper has presented an alternate method for characterizing nonlinear distortion from weakly nonlinear devices. The alternate method uses absorptive diplexers to separate the harmonic response from the high power probe signal, thus increasing the system's dynamic range. The method is also capable of measuring the reflected harmonic from devices. The method is relatively simple to implement and it is cost effective for measuring weak nonlinear responses of circuit elements. This paper has presented an implementation of this method with the capability of achieving 175-dBc dynamic range over a 22% bandwidth. The system is capable of producing over 10 W (+40 dBm) of probe signal power while measuring second harmonics generated by a DUT as low as −135 dBm, resulting in the 175 dBc dynamic range. This paper has outlined system requirements that dictate the dynamic range of the harmonic measurement system and provided guidance to achieve the required dynamic range. Results are presented on passive RF circuit elements that are not traditionally thought to exhibit nonlinearities, which require a high dynamic range, nonlinear measurement system.

Author Contributions: All authors equally conceived and designed the experiments; R.M.N. and K.A.G. performed the experiments; G.J.M. and A.F.M. provided the theoretical support; K.D.S. contributed the logistics and measurement facilities; all authors analyzed the data; R.M.N. wrote the first draft of the paper, and all authors contributed to its final form.

Funding: This research was supported by U.S. Army Research Office (ARO) contract #W911NF-12-1-0305 through a subcontract from Delaware State University (DSU).

Conflicts of Interest: The authors declare no conflict of interest. The funding sponsors had no role in the design of the study; in the collection, analyses, or interpretation of data; in the writing of the manuscript; or in the decision to publish the results.

References

1. Shitvov, A.; Schuchinsky, A.G.; Steer, M.B.; Wetherington, J.M. Characterisation of nonlinear distortion and intermodulation in passive devices and antennas. In Proceedings of the 8th European Conference on Antennas and Propagation (EuCAP), The Hague, The Netherlands, 6–11 April 2014; pp. 1454–1458.
2. Helme, B.G.M. Passive intermodulation of ICT components. In Proceedings of the IEE Colloquium on Screening Effectiveness Measurements, London, UK, 6 May 1998.
3. Golikov, V.; Hienonen, S.; Vainikainen, P. Passive intermodulation distortion measurements in mobile communication antennas. In Proceedings of the 54th IEEE Vehicular Technology Conference, Atlantic City, NJ, USA, 7–11 October 2001; pp. 2623–2625.
4. Belyaev, V.V.; Mayunov, A.T.; Razinkov, S.N. Effects of a metal insulator metal contact on the antenna in a radar monitoring system. *Meas. Technol.* **2001**, *44*, 871–875. [CrossRef]
5. Arazm, F.; Benson, F. Nonlinearities in metal contacts at microwave frequencies. *IEEE Trans. Electromagn. Compat.* **1980**, *22*, 142–149. [CrossRef]
6. He, H.; Fu, W. On passive intermodulation at microwave frequencies. In Proceedings of the Asia-Pacific Conference on Environmental Electromagnetics, Hangzhou, China, 4–7 November 2003; pp. 422–425.
7. Pedro, J.C.; Carvolho, N.B. *Intermodulation Distortion in Microwave and Wireless Circuits*; Artech House: Boston, MA, USA, 2003.
8. Giannini, F.; Leuzzi, G. *Nonlinear Microwave Circuit Design*; John Wiley & Sons: New York, NY, USA, 2004.
9. Martone, A.F.; Delp, E.J. Characterization of RF devices using two-tone probe signals. In Proceedings of the 2007 IEEE/SP Workshop on Statistical Signal Processing, Madison, WI, USA, 26–29 August 2007; pp. 161–165.

10. Gallagher, K.A.; Mazzaro, G.J.; Ranney, K.I.; Nguyen, L.H.; Martone, A.F.; Sherbondy, K.D.; Narayanan, R.M. Nonlinear synthetic aperture radar imaging using a harmonic radar. In Proceedings of the SPIE Conference on Radar Sensor Technology XIX, Baltimore, MD, USA, 20–22 April 2015; pp. 946109-1–946109-11.
11. Gallagher, K.A.; Narayanan, R.M.; Mazzaro, G.J.; Ranney, K.I.; Martone, A.F.; Sherbondy, K.D. Moving target indication with non-linear radar. In Proceedings of the IEEE Radar Conference, Arlington, VA, USA, 10–15 May 2015; pp. 1428–1433.
12. Mazzaro, G.J.; Martone, A.F.; McNamara, D.M. Detection of RF electronics by multitone harmonic radar. *IEEE Trans. Aerosp. Electron. Syst.* **2014**, *50*, 477–490. [CrossRef]
13. Colpitts, B.G.; Boiteau, G. Harmonic radar transceiver design: Miniature tags for insect tracking. *IEEE Trans. Antennas Propag.* **2004**, *52*, 2825–2832. [CrossRef]
14. Aumann, H.M.; Emanetoglu, N.W. A wideband harmonic radar for tracking small wood frogs. In Proceedings of the IEEE Radar Conference, Cincinnati, OH, USA, 19–23 May 2014; pp. 108–111.
15. Gallagher, K.A.; Narayanan, R.M.; Mazzaro, G.J.; Martone, A.F.; Sherbondy, K.D. Static and moving target imaging using harmonic radar. *Electronics* **2017**, *6*, 30. [CrossRef]
16. Wetherington, J.M.; Steer, M.B. Robust analog canceller for high-dynamic-range radio frequency measurement. *IEEE Trans. Microw. Theory Technol.* **2012**, *60*, 1709–1719. [CrossRef]
17. Bodson, M.; Sacks, A.; Khosla, P. Harmonic generation in adaptive feedforward cancellation schemes. *IEEE Trans. Autom. Control* **1994**, *39*, 1939–1944. [CrossRef]
18. Pedro, J.C.; De Carvalho, N.B. Evaluating co-channel distortion ratio in microwave power amplifiers. *IEEE Trans. Microw. Theory Technol.* **2001**, *49*, 1777–1784. [CrossRef]
19. Gallagher, K.A.; Mazzaro, G.J.; Narayanan, R.M.; Sherbondy, K.D.; Martone, A.F. Automated cancellation of harmonics using feed-forward filter reflection for radar transmitter linearization. In Proceedings of the SPIE Conference on Radar Sensor Technology XVIII, Baltimore, MD, USA, 5–7 May 2014; pp. 907703-1–907703-10.
20. Gallagher, K.A.; Narayanan, R.M.; Mazzaro, G.J.; Sherbondy, K.D. Linearization of a harmonic radar transmitter by feed-forward filter reflection. In Proceedings of the IEEE Radar Conference, Cincinnati, OH, USA, 19–23 May 2014; pp. 1363–1368.
21. Steer, M.B.; Khan, P.J. Large signal analysis of nonlinear microwave systems. In Proceedings of the 1984 IEEE International Microwave Symposium Digest, San Francisco, CA, USA, 30 May–1 June 1984; pp. 402–403.
22. Jakabosky, J.; Ryan, L.; Blunt, S. Transmitter-in-the-loop optimization of distorted OFDM radar emissions. In Proceedings of the IEEE Radar Conference, Ottawa, ON, Canada, 29 April–3 May 2013. [CrossRef]
23. Tjora, S.; Lundheim, L. Distortion modeling and compensation in step frequency radars. *IEEE Trans. Aerosp. Electron. Syst.* **2012**, *48*, 360–374. [CrossRef]
24. Ranta, T.; Ella, J.; Pohjonen, H. Antenna switch linearity requirements for GSM/WCDMA mobile phone front-ends. In Proceedings of the European Conference on Wireless Technology, Paris, France, 3–4 October 2005. [CrossRef]
25. Ko, B.K.; Cheon, D.B.; Kim, S.W.; Ko, J.S.; Kim, J.K.; Park, B.H. A nightmare for CDMA RF receiver: The cross modulation. In Proceedings of the First IEEE Asia Pacific Conference on ASICs, Seoul, Korea, 23–25 August 1999; pp. 400–402.
26. Moriya, A.; Inoue, M.; Kawachi, O. Development of high linearity duplexers with low passive intermodulation component. In Proceedings of the IEEE International Ultrasonics Symposium, Prague, Czech Republic, 21–25 July 2013; pp. 737–740.
27. Marttila, J.; Allen, M.; Kosunen, M.; Stadius, K.; Ryynanen, J.; Valkama, M. Reference receiver enhanced digital linearization of wideband direct-conversion receivers. *IEEE Trans. Microw. Theory Technol.* **2017**, *65*, 607–620. [CrossRef]
28. Ghadjati, M.; Moussaoui, A.K.; Bouchemel, A. Communication channel equalization based on Levenberg-Marquardt trained artificial neural networks. In Proceedings of the 3rd International Conference on Systems and Control, Algiers, Algeria, 29–31 October 2013. [CrossRef]
29. Rawat, M.; Roblin, P.; Quindroit, C.; Salam, K.; Xie, C. Concurrent dual-band modeling and digital predistortion in the presence of unfilterable harmonic signal interference. *IEEE Trans. Microwa. Theory Technol.* **2015**, *63*, 625–637. [CrossRef]
30. Chen, W.; Chen, X.; Zhang, S.; Feng, Z. Energy-efficient concurrent dual-band transmitter for multistandard wireless communications. In Proceedings of the Asia-Pacific Microwave Conference, Sendai, Japan, 4–7 November 2014; pp. 558–560.

31. Ding, L.; Hezar, R.; Erez, S. Modeling and predistortion for digital transmitters based on delta-sigma and pulse-width modulation. In Proceedings of the IEEE MTT-S International Microwave Symposium (IMS), San Francisco, CA, USA, 22–27 May 2016. [CrossRef]
32. Kechriotis, G.; Zervas, E.; Manolakos, E.S. Using recurrent neural networks for adaptive communication channel equalization. *IEEE Trans. Neural Netw.* **1994**, *5*, 267–278. [CrossRef] [PubMed]
33. Anritsu PIM PIM Master™ MW82119B. Available online: https://www.anritsu.com/en-US/test-measurement/products/mw82119b (accessed on 24 June 2018).
34. Kaelus Portable PIM Test Analyzers and Accessories. Available online: https://www.kaelus.com/en/test-measurement-solutions/portable-pim-testing (accessed on 24 June 2018).
35. Keysight N5249A PNA-X Microwave Network Analyzer, 8.5 GHz. Available online: https://www.keysight.com/en/pdx-x202055-pn-N5249A/pna-x-microwave-network-analyzer-85-ghz?cc=US&lc=eng (accessed on 24 June 2018).
36. Root, D.E.; Xu, J.; Horn, J.; Iwamoto, M.; Simpson, G. Device modeling with NVNAs and X-parameters. In Proceedings of the 2010 Workshop on Integrated Nonlinear Microwave and Millimeter-Wave Circuits, Göteborg, Sweden, 26–27 April 2010; pp. 12–15.
37. Keysight 2-Port and 4-Port PNA-X Network Analyzer. Available online: http://literature.cdn.keysight.com/litweb/pdf/N5242-90007.pdf (accessed on 24 June 2018).
38. Wilkerson, J.R.; Gard, K.G.; Steer, M.B. Automated broadband high-dynamic-range nonlinear distortion measurement system. *IEEE Trans. Microw. Theory Technol.* **2010**, *58*, 1273–1282. [CrossRef]
39. Wetherington, J.M.; Steer, M.B. Characterization of the dynamic range of a single aperture communications system. In Proceedings of the 2012 Workshop on Integrated Nonlinear Microwave and Millimetre-Wave Circuits (INMMIC), Dublin, Ireland, 3–4 September 2012. [CrossRef]
40. Walker, A.L. Behavioral Modeling and Characterization of Nonlinear Operation in RF and Microwave Systems. Ph.D. Thesis, North Carolina State University, Raleigh, NC, USA, 2005.
41. Maas, S.A. *Nonlinear Microwave Circuits*, 2nd ed.; Artech House: New York, NY, USA, 1988.
42. Martone, A.F. Forensic Characterization of RF Circuits. Ph.D. Thesis, Purdue University, West Lafayette, IN, USA, 2007.
43. Mazzaro, G.J. Time-Frequency Effects in Wireless Communication Systems. Ph.D. Thesis, North Carolina State University, Raleigh, NC, USA, 2009.
44. Gallagher, K.A.; Mazzaro, G.J.; Martone, A.F.; Sherbondy, K.D.; Narayanan, R.M. Derivation and validation of the nonlinear radar range equation. In Proceedings of the SPIE Conference on Radar Sensor Technology XX, Baltimore, MD, USA, 18–21 April 2016; pp. 98290P-01–98290P-13.
45. National Instruments PXIe-5668 PXI Vector Signal Analyzer. Available online: http://www.ni.com/en-us/support/model.pxie-5668.html (accessed on 24 June 2018).
46. Peng, Z.; Psychogiou, D.; Li, C. Investigation of the roles of filters for a harmonic FMCW radar. In Proceedings of the 2017 International Applied Computational Electromagnetics Society Symposium (ACES), Suzhou, China, 1–4 August 2017; pp. 1–2.
47. National Instruments RF and Microwave Signal Generators. Available online: http://www.ni.com/white-paper/3994/en/ (accessed on 24 June 2018).
48. Gallagher, K.A.; Mazzaro, G.J.; Martone, A.F.; Sherbondy, K.D.; Narayanan, R.M. Filter selection for a harmonic radar. In Proceedings of the SPIE Conference on Radar Sensor Technology XIX, Baltimore, MD, USA, 20–22 April 2015; pp. 94610A-01–94610A-11.
49. Young, L. Microwave filters—1965. *IEEE Trans. Microw. Theory Technol.* **1965**, *13*, 489–508. [CrossRef]
50. Hoffman, M. Microwave diplexer. *Electr. Commun.* **1970**, *45*, 358–362.
51. Macchiarella, G.; Tamiazzo, S. Novel approach to the synthesis of microwave diplexers. *IEEE Trans. Microw. Theory Technol.* **2006**, *54*, 4281–4290. [CrossRef]
52. Messenger, G.C.; McCoy, C.T. Theory and operation of crystal diodes as mixers. *Proc. IRE* **1957**, *45*, 1269–1283. [CrossRef]
53. Miura, T.; Davis, L.E. A study of ferrite nonlinearity evaluation from higher harmonic generation efficiency. In Proceedings of the 2006 European Microwave Conference, Manchester, UK, 10–15 September 2006; pp. 917–920.

54. Bayrak, M.; Benson, F.A. Intermodulation products from nonlinearities in transmission lines and connectors at microwave frequencies. *Proc. IEE* **1975**, *122*, 361–367. [CrossRef]
55. Zhang, K.; Li, T.; Jiang, J. Passive intermodulation of contact nonlinearity on microwave connectors. *IEEE Trans. Electromagn. Compat.* **2018**, *60*, 513–519. [CrossRef]